JOURNAL OF CATALYSIS 149, 326–343 (1994)

Vanadia–Titania Aerogels

I. Preparation, Morphological Properties, and Activity for the Selective Catalytic Reduction of NO by NH_3

M. Schneider,* M. Maciejewski,* S. Tschudin,* A. Wokaun,† and A. Baiker*,[1]

*Department of Chemical Engineering and Industrial Chemistry, Swiss Federal Institute of Technology, ETH-Zentrum, CH-8092 Zürich Switzerland, and †Physical Chemistry II, University of Bayreuth, D-95440 Bayreuth, Germany

Received February 15, 1994; revised May 24, 1994

Highly dispersed vanadia–titania aerogels with high surface area have been synthesized by a two-stage sol–gel process with ensuing high-temperature supercritical drying. A titania gel was prepared by the addition of an acidic hydrolysant to tetrabutoxytitanium(IV) in methanolic solution. The vanadium alkoxide precursor was added after redispersing the titania gel. The influences of different preparation conditions on the morphological and chemical properties of the aerogels were studied. The aerogels were characterized by means of nitrogen physisorption, X-ray diffraction, transmission electron microscopy, and thermal analysis (thermogravity, differential thermal analysis) coupled with mass spectrometry. The meso- to macroporous vanadia–titania aerogels possess a BET surface area of 140 to 220 $m^2 g^{-1}$ after calcination up to 673 K and contain well-developed anatase crystallites of ca. 10 nm mean size. Crystalline V_2O_5 was detected only for samples calcined at 723 K. All other aerogel catalysts, calcined at lower temperature, showed no indication for long-range ordered vanadia domains. Thermal analysis revealed that even calcination at 723 K was not sufficient for complete removal of organic residues, which were entrapped during supercritical drying. The catalytic properties of the aerogels were tested for the selective catalytic reduction of NO by NH_3. An increase in the vanadia loading from 5 to 30 wt% V_2O_5 resulted in a marked increase in overall as well as specific activity, whereas the apparent activation energy decreased from 66 to 55 kJ mol^{-1}. An increase in the calcination temperature from 573 to 673 K led to a significant rise in the activity of the vanadia–titania aerogel catalyst. The aerogel with 30 wt% V_2O_5 showed a reaction rate referred to the vanadium content (turnover frequency) that is similar to that of multiply grafted well-dispersed vanadia/titania catalysts. Among all catalysts presented in this work, this aerogel exhibited the highest reaction rate per gram of catalyst.

INTRODUCTION

Aerogel catalysts offer unique morphological and chemical properties (1–3). These properties originate from their wet-chemical preparation by the solution–sol–gel (SSG) method (4) and the subsequent removal of solvent by supercritical drying (SCD). As this "gentle" drying procedure is capable of "preserving" the structural properties of an open gel network (5), the aerogels are usually solids of large porosity and specific surface area.

Vanadia-based catalysts (6) are used for various processes such as the selective catalytic reduction of NO by NH_3, ammoxidation of aromatic hydrocarbons, and partial oxidation reactions. Several methods have been applied for the preparation of vanadia/titania catalysts, including impregnation (6), selective grafting from nonaqueous solutions (6–8) or by chemical vapor deposition (6, 9), mechanical mixing of V_2O_5 and TiO_2 (6), coprecipitation (6), sequential precipitation (10), as well as SSG processes based on metal alkoxide precursors (11, 12).

The coupling of the sol–gel process with supercritical drying offers the combination of the intrinsic advantages of the SSG method (dispersion, homogeneity, molecular mixing) with the favorable textural characteristics of aerogels. Such a direct SSG preparation of a binary oxide–oxide solid with high dispersion and accessibility of the active component requires careful control of the preparation conditions and knowledge of the sol–gel reactivity of the metal alkoxides used.

In a recent survey, Livage (13) reports on the chemical, structural, and electrical properties as well as the intercalation and ion-exchange behavior of differently prepared V_2O_5 (aqueous and alkoxidic SSG route). Nabavi *et al.* (14) investigated the hydrolysis and polycondensation of

[1] To whom correspondence should be addressed.

0021-9517/94 $6.00

different vanadium alkoxides with respect to dependence on the hydrolysis level, i.e., $mol_{H_2O} : mol_{alkoxide}$. They showed that the nature of the resulting material varies significantly. Hydrolysis levels smaller than the stoichiometric amount led to the production of polymeric oxo species with incorporated organic groups. Such xerogels are generally X-ray amorphous after drying at ambient conditions. An aqueous gel is obtained by a large water excess, leading to a layered structure similar to V_2O_5 prepared by aqueous polycondensation of vanadic acid. Hirashima *et al.* studied the synthesis of vanadia xerogels (15, 16) and aerogels (17, 18). Sudoh and Hirashima (18) demonstrated the preparation of vanadia aerogels with about 200 $m^2 g^{-1}$ surface area by hydrolysis of vanadium oxide triethoxide in ethanol and subsequent high-temperature supercritical drying. The resulting aerogels were black due to the reduction by the supercritical alcohol. Based on their systematic studies on the effects of hydrolysis level, alkoxide concentration, alkoxide type, and pH (15), the authors demonstrated the regimes in which sols, precipitates, or monolithic gels are formed. Addition of acid usually increases the rate of hydrolysis and decreases the gelation, i.e., polycondensation. On modification of the alkoxide ligands, the hydrolysis rate decreased in the order ethoxide, butoxide, and isopropoxide (15). The hydrolysis rate decreases with increasing steric hindrance of the alkoxide ligands, which is a common property of many other alkoxide systems (4). This behavior implies that small, linear, easily hydrolyzable alkoxide ligands together with an acidic sol–gel medium seem to fulfill the requirements for forced hydrolysis. Consequently, nucleation dominates over particle growth, which leads to high dispersity.

As already mentioned, among the many SCR catalysts studied (19), vanadia–titania is still the one that is most widely used. Commercial TiO_2 with 50 $m^2 g^{-1}$ (e.g., P25 Degussa) is frequently employed as support material. Recently we succeeded in preparing a meso- to macroporous titania aerogel with a BET surface area of nearly 200 $m^2 g^{-1}$ (20). The crystalline part of this titania consists of well-developed anatase crystallites. The procedure for preparation of this material offers an interesting alternative to the commercial titania prepared by flame hydrolysis. With this in mind, we developed a method for the direct synthesis of vanadia–titania aerogels. Instead of mixing titanium and vanadium alkoxides at the beginning of the SSG process, we tried to return to the "primary" structure of the titania matrix via redispersion of titania gels. This procedure provides the advantage of homogeneously dispersing the vanadium precursor in the SSG sample. Another beneficial aspect arises from the use of preformed "colloidally" dispersed titania, which helps to prevent the incorporation of the active vanadium constituent.

TABLE 1

Aerogel Designations and Corresponding Preparation Conditions[a]

Solution–sol–gel stage		Supercritical drying stage	
Aerogel	*Varied parameter*	Aerogel	*Varied parameter*
V20*STA*	'V_2O_5'[b] 20 wt% (18.0 at.%) STAndard		
	Calcination Temperature		Heating Rate
V20*STA*623[c]	623 K	V20*HR*8	8 K h^{-1}
V20*STA*673[c]	673 K	V20*HR*30	30 K h^{-1}
V20*STA*723[c]	723 K	V20*HR*120	120 K h^{-1}
	Vanadium alkoxide		
V20*ViP*	$VO(i\text{-}OPr)_3$		
	Sol–Gel Temperature		Pressure-release Rate
V20*SGT*273	273 K	V20*PR*3	3 MPa h^{-1}
V20*SGT*323	323 K	V20*PR*12	12 MPa h^{-1}
	Hydrolysis catalyst		
V20*H2SO4*	H_2SO_4		
	'V_2O_5'[b] loading		Extra Methanol
*V*0	0 wt%	V20*EM*0	0 ml
*V*5	5 wt% (4.4 at.%)		
*V*10	10 wt% (8.9 at.%)		Nitrogen Prepressure
*V*30	30 wt% (27.4 at.%)	V20*NP*10	10 MPa
*V*100	100 wt%		

[a] Those conditions that deviate from the standard synthesis procedure.

[b] The amount of vanadia is calculated on the basis of nominal vanadium(V) pentoxide ('V_2O_5').

[c] Calcination temperature studies were carried out with portions of the raw standard aerogel V20*STA*.

In this work a direct route for the preparation of vanadia–titania aerogels with high dispersion and accessibility of the active vanadia component, as well as catalytically favorable textural properties, is shown. The influence of crucial wet-chemical and supercritical drying conditions on the structural and chemical properties of vanadia–titania aerogels was investigated, and their catalytic performance in the selective catalytic reduction (SCR) of NO by NH_3 was tested.

EXPERIMENTAL

Sol–Gel–Aerogel Synthesis

Throughout the article a set of acronyms for the individual aerogels is used. A survey of the aerogel designations and corresponding preparation conditions, i.e., those conditions that deviate from the standard synthesis procedure, is given in Table 1.

Standard synthesis. Analytical-grade reagents were used throughout this work. The preparation of the titania gels followed basically that of aerogel C in (20). In brief, the SSG process was carried out in an antiadhesive, closed Teflon beaker, under nitrogen atmosphere and at ambient temperature (297 ± 2 K). Two solutions were prepared.

The first solution consisted of 32.0 g of tetrabutoxytitanium(IV) (TBOT) dissolved in 120 ml methanol, and the second of 6.78 ml bidistilled water and 0.52 ml nitric acid (65 wt%) in 30 ml methanol. The latter was added to the TBOT solution in a closed, initially nitrogen-flushed system under vigorous stirring (ca. 1000 rpm). The as-prepared, translucent gels (gelation time 2–3 min) were aged 4 h to increase the rigidity of the gel network by successive polycondensation reactions. After this first aging process the titania gels were redispersed under ambient atmosphere with 72 ml extra methanol and a glass rod, to favor a homogeneous distribution of the vanadium alkoxide. The suspension was homogenized for 10 min again under nitrogen atmosphere and reduced stirring (ca. 500 rpm). An opaque, nonviscous solution resulted. Then 5.0 g vanadium(V) oxide tri-*n*-propoxide (VOTP) diluted in 18.6 ml methanol was introduced by syringe. After a second aging step of additional 4 h under vigorous stirring, 1.12 ml of bidistilled water diluted in 4.5 ml methanol was added in the same way, to adjust the stoichiometric hydrolysis level. The corresponding overall molar ratio, H_2O : (TBOT + VOTP) : HNO_3, was 3.94 : 1 : 0.065. The orange translucent solution was stirred vigorously for another 15 h.

To exceed the critical conditions without formation of a vapor–liquid interface inside the pores (5), the sol–gel product as described above was transferred in a stainless-steel liner into an autoclave with a net volume of 1.09 liters together with 130 ml of additional methanol (outside of the liner), to give ca. 375 ml in all cases, thus surpassing the critical volume of the mixed solvent. The corresponding critical data for methanol, as the dominating component of all SSG solvents used here, are V_c = 118 ml mol^{-1}, T_c = 513 K, and p_c = 8.1 MPa (21). The high-pressure system was flushed with nitrogen, pressurized to 5 MPa, hermetically closed, and heated with a temperature ramp of 1 K min^{-1} to 533 K. The autoclave was kept at the final temperature for 30 min to ensure complete thermal equilibration. The final pressure was about 19 MPa. Then the pressure was released isothermally at 0.1 MPa min^{-1}. The system was flushed with nitrogen and allowed to cool to ambient temperature. The resulting violet-black aerogel clumps were ground in a mortar. The color indicated a strongly reduced oxidation state of the vanadium component [vanadium(III) sesquioxide, black; vanadium(IV) dioxide, blue; vanadium(V) pentoxide, orange], as presented previously (18).

Finally, a portion of the uncalcined (raw) aerogel powder was calcined in a tubular reactor with upward flow. The temperatures given corresponded to the oven temperature. GHSV amounted to ca. 1000 h^{-1} (ca. 3 g aerogel sample). To remove most of the organic residues prior to calcination, all aerogel samples were first pretreated in a purified nitrogen flow of 0.5 liters min^{-1} at 573 K for 1 h. After being cooled to about 353 K in nitrogen and heated again at 5 K min^{-1}, this time in air flowing at 0.5 liters min^{-1}, the portion of the raw aerogel was calcined for another 5 h at 573 K. The color turned from violet-black to brown-green.

The loadings are expressed by weight percent of nominal vanadium(V) pentoxide ('V_2O_5') throughout the text. They are generally calculated on the basis of the weighted amounts, assuming a theoretical stoichiometry 'V_2O_5–TiO_2'. Such a description, especially in the case of the vanadia component, implies a slight systematic error. The stoichiometry is not exactly V_2O_5, as will be shown later. Therefore, atom percentages of vanadium are given in Table 1. The contents in atom percentages of vanadium and thus nominal weight percentages 'V_2O_5' were independently confirmed by thermogravimetry (oxidation–reduction cycles).

In the following subsections more detailed information is given for the single preparation condition series investigated. In general, the conditions varied and their effects are pointed out.

Calcination temperature. Portions of V20*STA*, the standard aerogel, were used for the calcination investigations. The thermal pretreatments were carried out as described above, with the calcination temperature changed to 623, 673, or 723 K.

Sol–gel temperature. Additional preparations were performed with the wet-chemical sol–gel temperature adjusted to 273 and 323 K (both with a certainty of ±2 K). Prior to use, all solutions were thermally equilibrated at the specified temperatures. At 273 K a white titania suspension developed; at 323 K a titania gel formed immediately. The additional procedure followed the standard one.

Hydrolysis catalyst. Nitric acid (hydrolysis catalyst) was replaced by 0.4 ml sulfuric acid (95–97 wt%), resulting in the same molarity. The use of sulfuric acid did not lead to gelation; on the contrary a white suspension developed. No extra methanol and a nitrogen prepressure of 10 MPa were used for the SCD, which resulted in a final pressure of ca. 26 MPa. A gray, sticky powder was obtained. Further processing was as stated above (standard synthesis).

Vanadia loading. As mentioned, the loading was varied based on theoretical weight percentages of 'V_2O_5'. After redispersion of the titania gel the desired quantity of VOTP was added. The quantities that were changed in the corresponding preparations for *V*0 to *V*30 are summarized in Table 2. The additional procedure followed the standard one. With *V*30 a highly viscous solution developed on addition of the VOTP solution.

With *V*100 two solutions were prepared. The first solution consisted of 22.8 g VOTP in 165 ml methanol, and the second of 20.1 ml bidistilled water and 0.52 ml nitric acid in 80 ml methanol. The latter was added to the VOTP

TABLE 2

Changes in the Preparation Conditions for Varying the Vanadia Loading

Aerogel	Methanol used for redispersion (ml)[a]	VOTP (g) in methanol (ml)[b]		Hydrolysant: H_2O (ml) in methanol (ml)[c]	
*V*0	72	0	18.6	0	4.5
*V*5	90	1.05	4	0.24	1
*V*10	85	2.2	8.2	0.5	2
*V*30	56	8.6	31.4	1.91	7.6

[a] Amount of methanol used for redispersion of the titania gel.
[b] Composition of vanadium oxide *tri-n-propoxide* (VOTP) precursor solution.
[c] Composition of the hydrolysant "completing" the stoichiometric hydrolysis of VOTP.

solution. An orange suspension developed, which turned transparent red after ca. 10 min. The as-prepared vanadia sol was aged 19 h and, at last, supercritically dried at 538 K instead of 533 K (final pressure ca. 20 MPa). Note the increased water content, which led to that slight increase in the SCD temperature due to the higher critical temperature of water, T_c = 647 K (22). A black powder was obtained. The strongly reduced state after SCD became apparent in the marked exothermicity after exposure to air (especially with *V*30 and *V*100).

Nitrogen prepressure and extra amount of methanol for SCD. To exceed the critical state without formation of a vapor–liquid interface inside the pores (5), thus avoiding detrimental differential capillary forces, the total amount of methanol needed is commonly derived from the specific critical volume of the solvent together with the void volume of the autoclave. Mulder and van Lierop (23), however, showed that such a prerequisite can be circumvented by applying an inert-gas prepressure, by which possible bubble formation due to temperature inhomogeneities can be suppressed as a consequence of the increased total system pressure (23). V20*EM*0 and V20*NP*10 were thus supercritically dried with nitrogen prepressures of 5 and 10 MPa, respectively, and no extra methanol (total methanol ca. 245 ml). The additional processing was as stated above (standard synthesis). The final pressures amounted to ca. 16 and 24 MPa, respectively.

Physicochemical Characterization

Nitrogen physisorption. The Specific surface areas (S_{BET}), mean cylindrical pore diameters ($\langle d_p \rangle$), and specific adsorption pore volumes (V_{pN_2}) were obtained from nitrogen physisorption at 77 K using a Micromeritics ASAP 2000 instrument. Prior to measurement, all samples were degassed to 0.1 Pa at 423 K. BET surface areas were calculated in a relative pressure range of 0.05 to 0.2, assuming a cross-sectional area of 0.162 nm^2 for the nitrogen molecule. The pore size distributions were calculated by applying the Barrett–Joyner–Halenda method (24) to the desorption branches of the isotherms (25). The assessments of microporosity were made from *t*-plot constructions ($0.3 < t < 0.5$ nm, calcined aerogels; $0.5 < t < 0.8$ nm, raw aerogels), using the Harkins–Jura correlation (26).

X-ray diffraction. X-ray powder diffraction (XRD) patterns were measured on a Siemens Θ/Θ D5000 powder X-ray diffractometer. The diffractograms were recorded with Cu$K\alpha$ radiation over a 2Θ range of 10° to 80°. The detector used was either a position-sensitive detector with Ni filter or, in the case of poorly crystalline samples, a scintillation counter with secondary monochromator. The mean crystallite sizes were determined from the Scherrer equation with the normal assumption of spherical crystallites (27) and the (200) or (101) reflection (only in the presence of crystalline V_2O_5) for anatase (28), the (110) reflection for rutile (29), and the (001) (only with V100) or (400) reflection for crystalline V_2O_5 (shcherbinaite) (30), using the Split Pearson7 fit function.

Transmission electron microscopy. Samples for transmission electron microscopy (TEM) were loaded dry onto perforated, thin carbon films supported on copper grids, aerogel powder being poured five times onto the carbon film and shaken off.

Diffraction-contrast TEM was performed using a Hitachi H-600 electron microscope operated at 100 kV, with a point resolution of about 0.5 nm. The instrumental magnification had previously been calibrated, using the phase contrast from catalase crystals. High-resolution, phase-contrast TEM was carried out on a Philips CM30ST electron microscope at 300 kV, with a point resolution of 0.19 nm. Here the 0.352-nm lattice fringes from anatase were employed as an internal calibrant of the magnification.

Thermal analysis. Thermogravimetry (TG) and differential thermal analysis (DTA) were performed on a Netzsch STA 409 coupled with a Balzers QMG 420 quadrupole mass spectrometer, equipped with Pt–Rh thermocouples and Pt crucibles. A heating rate of 10 K min^{-1} and an air flow of 25 ml min^{-1} were used. The sample weight was 50–100 mg, and the α-Al_2O_3 reference weight, 60–80 mg.

Total carbon and hydrogen contents were determined with a LECO CHN-900 elemental microanalysis apparatus. Total sulfur content was determined by Schöniger decomposition (31) and subsequent ion chromatography.

Selective Catalytic Reduction of NO by NH_3

Catalyst testing for the selective catalytic reduction of NO by NH_3 was performed in a quartz tube fixed-bed microreactor with 4-mm inner diameter. Reactant and

product gases were analyzed on line with a quadrupole mass spectrometer (Balzers QMG420/QMA120). Prior to catalytic testing the aerogel powders were agglomerated at 2 MPa for 1 min. These conditions proved to be sufficient to yield fairly stable granules, leaving the textural properties virtually unchanged. The reactor bed consisted of 44-mg granules (120–300 μm) with a constant bed volume of 0.126 cm^3 and a constant bed height of 1 cm. Exceptions are explicitly stated. The simulated stack emission feed consisted of 900 vppm NO and NH_3 and 1.8 v% O_2, with argon being the balance gas. Prior to catalytic runs the aerogel catalysts were pretreated in 7 v% O_2–Ar at 573 K for 1 h and then exposed to SCR reactant gas at 423 K for another hour. Routine testing involved an integral reactor test and a differential reactor test. In the former, the product yields of N_2 and N_2O were studied under steady-state conditions by increasing catalyst temperature at a constant space velocity of ca. 24,000 h^{-1} (273.15 K, 1 atm, STP). Differential reactor tests were performed between 372 and 470 K for space velocities of 17,000–100,000 h^{-1} (STP), while maintaining conversion at 17–22%.

Preliminary tests with greatly different granule fractions of the standard aerogel V20*STA* showed that the kinetic data determined between 395 and 440 K were independent of particle size (<500 μm), indicating that internal mass transfer influences could be ruled out. However, a rough estimate, using the criterion of Weisz and Prater, $(-r)_{obs} L^2/(D_e C_g) < 1$, for negligible pore resistance (32), yielded a value of 2 for V20*STA* (470 K, 0.1 MPa), suggesting that at temperatures of ca. 470 K and higher, pore diffusion effects could become influential. For that reason the majority of the kinetic tests were run at temperatures lower than 440 K.

The experimental error of the catalytic testing was estimated from three consecutive measurements with V20*STA*. The resulting experimental error was ca. 10%. The linear regression errors of the apparent activation energies calculated from the corresponding Arrhenius analysis amounted to 1–5%. Repetitive preparations of selected aerogels showed that the materials could be well reproduced and yielded activities that differed by less than 6%.

RESULTS

Morphological and chemical properties of both the calcined aerogel catalysts and their parent raw aerogels are listed in Table 3.

Physicochemical Characterization

Nitrogen physisorption. Caution must be exerted when interpreting absolute physisorption data derived from such highly structured aerogels (33). Usually the specific pore volumes (V_{pN_2}) measured are too low in the light of the appropriate bulk densities. Obviously the largest pores, which contribute most to V_{pN_2}, are not detected by nitrogen physisorption. Nevertheless, comparisons within a series of similarly prepared materials are meaningful.

Figure 1 depicts the adsorption/desorption isotherms, the differential pore size distribution derived from the desorption branch (25), and the *t*-plot (top left) for the V20*STA* sample, calcined in air at 573 K. These features are representative of all binary aerogels calcined at 573–673 K (excluding V20*H2SO4*, synthesized with sulfuric acid). They all show a type IV isotherm with an H1 desorption hysteresis according to IUPAC classification (34) and pronounced meso- to macroporosity with only little microporosity. The specific micropore surface areas, estimated from the corresponding *t*-plot analysis, amounted to ≤ 13 $m^2 g^{-1}$. They possess S_{BET} of 173 to 220 $m^2 g^{-1}$, V_{pN_2} of 0.87 to 1.11 $cm^3 g^{-1}$, and very broad, asymmetric pore size distributions (Fig. 1). The latter feature also emerges from comparison of the pore size maxima (ca. 50 nm, Fig. 1) with the mean cylindrical pore sizes $<d_p>$ given in Table 3. Only the V20*ViP* sample (synthesized with vanadium oxide tri-isopropoxide) and the V20*HR*8 sample (prepared with the slowest heating rate), both calcined at 573 K, show significantly lower S_{BET} of 157 and 152 $m^2 g^{-1}$, respectively. For comparison, raw V20*HR*8 has a BET surface area of 182 $m^2 g^{-1}$. The textural properties of a raw aerogel (degassed at 423 K) are exemplified by the uncalcined V20*STA*, which is characterized by an S_{BET} of 212 $m^2 g^{-1}$, a V_{pN_2} of 0.98 $cm^3 g^{-1}$, and a specific micropore surface area of 24 $m^2 g^{-1}$ (derived from the corresponding *t*-plot shown in Fig. 1, top right). The *t*-plot with its reduced adsorption capacity at low relative pressures is characteristic of the raw aerogel materials, suggestive of some weak interaction of the adsorptive (N_2) with the raw aerogels covered by organic residues (see thermoanalytical studies below). Comparison with data for the catalyst V20*STA* calcined at 573 K (Table 3) reveals that the calcination causes mainly a loss in microporosity, but otherwise the textural properties are almost preserved.

With respect to the influence of calcination temperature, it emerges from Table 3 that calcination at 723 K (V20*STA*723) leads to a drastic decline in both S_{BET} (42 $m^2 g^{-1}$) and V_{pN_2} (0.38 $cm^3 g^{-1}$; see X-ray diffraction studies presented below). This calcination virtually eliminates pores smaller than ca. 10 nm, but preserves the meso- to macroporous network.

Figure 2a depicts the adsorption/desorption isotherms and the differential pore size distribution derived from the desorption branch (25) for V20*H2SO4*, prepared with sulfuric acid and calcined at 573 K. It shows a type IV isotherm with an H1–H3 desorption hysteresis (34), which

TABLE 3

Morphological and Chemical Properties of Both the Aerogel Catalysts Calcined in Flowing Air at 573 K (Excluding the Calcination Series V20*STA*623, V20*STA*673, V20*STA*723) and Their Raw Parent Aerogels

Aerogel	S_{BET} (S_t)[a] (m^2/g)	$\langle d_p \rangle$ (nm)[b]	V_{pN_2} (cm^3/g)	XRD crystallinity and $\langle d_c \rangle$ (nm)[c]			Carbon content (wt%)[d]
V20*STA*	192(11)	21	1.00	A	7.3	(6.5)	2.2
V20*STA*623	202(10)	21	1.06	A	7.0	(6.5)	2.2
V20*STA*673	178(8)	23	1.01	A	7.2	(6.5)	2.2
V20*STA*723	42(2)	36	0.38	A, R, S	18, 40, 22	(6.5)	2.2
V20*ViP*	157(10)	25	0.97	A	8.9	(6.4)	2.3
V20*SGT*273	173(9)	23	1.00	A	8.9	(6.5)	2.0
V20*SGT*323	191(13)	20	1.04	A	7.5	(7.3)	1.5
V20*H2SO4*	134(8)	22	0.74	A	9.0	(8.9)	1.2 (2.1)
*V*0	182(13)	16	0.71	A	7.4	(7.4)	1.3
*V*5	194(10)	20	0.95	A	7.3	(7.0)	2.8
*V*10	183(11)	20	0.93	A	7.5	(6.5)	2.5
*V*30	195(7)	22	1.09	A	13	(13)	1.6
*V*100	25(1)	27	0.16	S; V	18, 16; —	(—)	0.57
V20*HR*8	152(9)	26	0.97	A	9.7	(7.0)	2.2
V20*HR*30	196(12)	19	0.95	A	7.0	(6.5)	2.8
V20*HR*120	181(9)	20	0.88	A	7.9	(6.1)	2.6
V20*PR*3	208(12)	21	1.08	A	6.6	(6.5)	2.8
V20*PR*12	199(13)	20	0.87	A	7.0	(6.5)	2.4
V20*EM*0	201(11)	20	0.99	A	8.0	(6.3)	2.7
V20*NP*10	220(12)	20	1.11	A	6.5	(6.3)	2.7

[a] S_t in parentheses is specific micropore surface area derived from *t*-plot analysis.

[b] $\langle d_p \rangle = 4V_{pN_2}/S_{BET}$.

[c] A (anatase), R (rutile), S (shcherbinaite, V_2O_5), V (vanadium(IV) oxide, most likely VO_2 and/or V_2O_4) in order of decreasing intensity; $\langle d_c \rangle$ corresponding mean crystallite sizes (—, not determinable), in parentheses the values of the raw aerogels.

[d] Carbon content (in parentheses sulfur content) of the raw aerogels determined by elemental microanalysis.

results in an almost bimodal pore size distribution with a symmetric, narrow mode at ca. 20 nm. The specific surface area of 134 $m^2\ g^{-1}$ is the lowest value obtained among the vanadia–titania aerogels calcined at 573 K.

Textural characteristics of the pure vanadia aerogel *V*100, both raw and calcined at 573 K, are illustrated in Fig. 2b. They both have a type IV isotherm and an H1–H3 desorption hysteresis (34), again indicative of bimodal differential pore size distributions. Calcination at 573 K shifts the hysteresis to higher relative pressures, and consequently the two pore size modes are shifted to larger pore sizes, i.e., from ca. 6 and 20 nm to ca. 15 and 60 nm. In addition, the specific surface area decreased drastically from 80 to 25 $m^2\ g^{-1}$ (see X-ray diffraction studies below) and the specific pore volume dropped from 0.25 to 0.16 $cm^3\ g^{-1}$. The specific micropore surface area remained virtually unaltered (3 and 1 $m^2\ g^{-1}$, respectively).

X-ray diffraction (XRD). Vanadia–titania aerogels, both raw and calcined at 573–673 K, contain well-developed anatase crystallites (28) of mean sizes 6.1–8.9 nm (without V20*H2SO4*, 6.1–7.4 nm) and 6.5–9.7 nm, respectively, as indicated in Table 3. Calcination generally causes an increase of the mean crystallite size, often, however, within the precision of the line-broadening analysis. Only the aerogel with the highest vanadia loading, *V*30 (30 wt% 'V_2O_5'), contains significantly larger anatase crystallites of mean size 13 nm. Table 3 also indicates that the vanadia component of all binary aerogels is X-ray amorphous up to 673 K.

The X-ray patterns of the V20*STA* series, both raw and after calcination at different temperatures, are shown in Fig. 3. It is apparent that up to 673 K (patterns a–d) neither the crystallinity of anatase changed nor did crystalline vanadium oxide (20 wt% 'V_2O_5') become detectable. At 723 K, however, crystalline V_2O_5 (30) evolved, and concomitantly a part of the anatase phase topotactically transformed into rutile (29), resulting in a rutile-to-anatase ratio of ca. 0.31 (35–37) (Fig. 3). Thus, the V20*STA*723 sample (calcined at 723 K) consists of highly crystalline anatase, rutile, and shcherbinaite with mean crystallite sizes of 18,

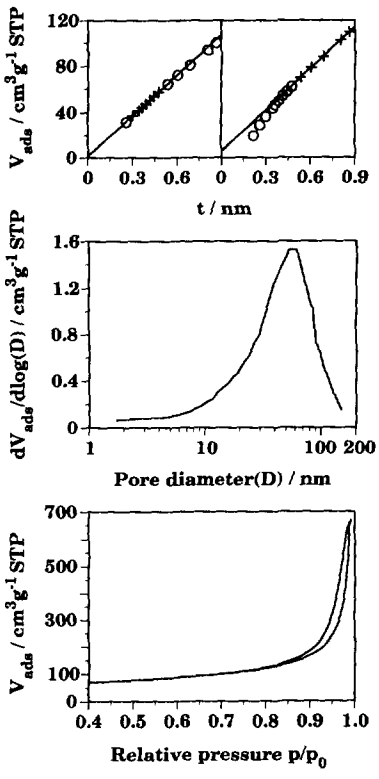

FIG. 1. Textural properties of aerogel V20*STA* calcined at 573 K in air (standard). Bottom: adsorption/desorption isotherms (STP, 273.15 K, 1 atm); middle: differential pore size distribution derived from the desorption branch of nitrogen physisorption; top left: *t*-plot of the calcined aerogel (+, linear regression points); top right: *t*-plot of the raw aerogel (+, linear regression points).

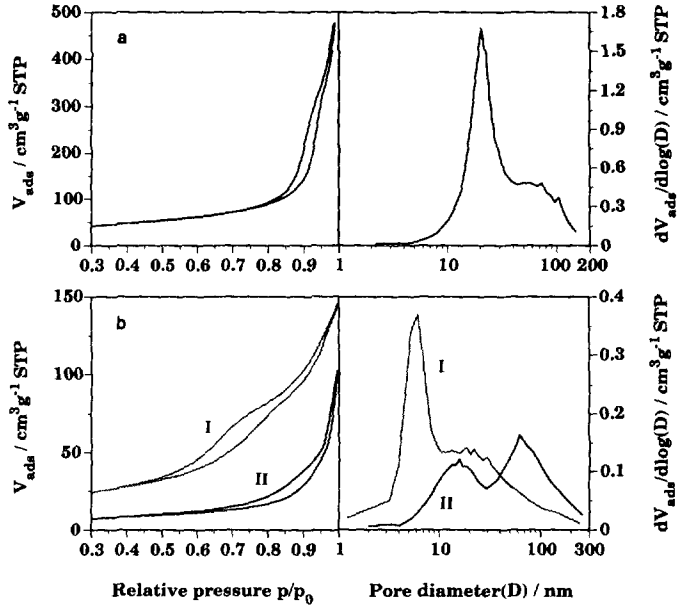

FIG. 2. Nitrogen physisorption (STP, 273.15 K, 1 atm) on aerogels (a) V20*H2SO4* calcined at 573 K in air and (b) *V*100 (I for the raw aerogel, II after calcination at 573 K). Designations of aerogels are explained in Table 1.

40, and 22 nm, respectively (Table 3). These transformations were accompanied by a loss of specific surface area and specific pore volume (Table 3).

Figure 4 represents the XRD patterns of the vanadia aerogel *V*100, both raw and calcined at 573 K. It is obvious that high-temperature supercritical drying led to marked reduction of the vanadia aerogel, showing crystalline vanadium(IV) oxide [mostly likely VO_2 and/or V_2O_4 (38)] as the main phase together with V_6O_{13} (39) and traces of V_2O_5 (30) (pattern a). However, calcination at 573 K reoxidized most of the vanadia component to crystalline V_2O_5, with a residual of vanadium(IV) oxide. As already stated in the section on physisorption, this oxidation–recrystallization resulted in a significant decrease in both the specific surface area and the specific pore volume (Table 3).

Transmission electron microscopy (TEM). A representative TEM image from a portion of V20*STA* calcined at 573 K is given in Fig. 5. The ultrastructure of branched and interconnected colloidal primary particles, which form ultrafine cells (<100 nm), is characteristic of aerogel materials. The high-resolution TEM image in Fig. 6 re-

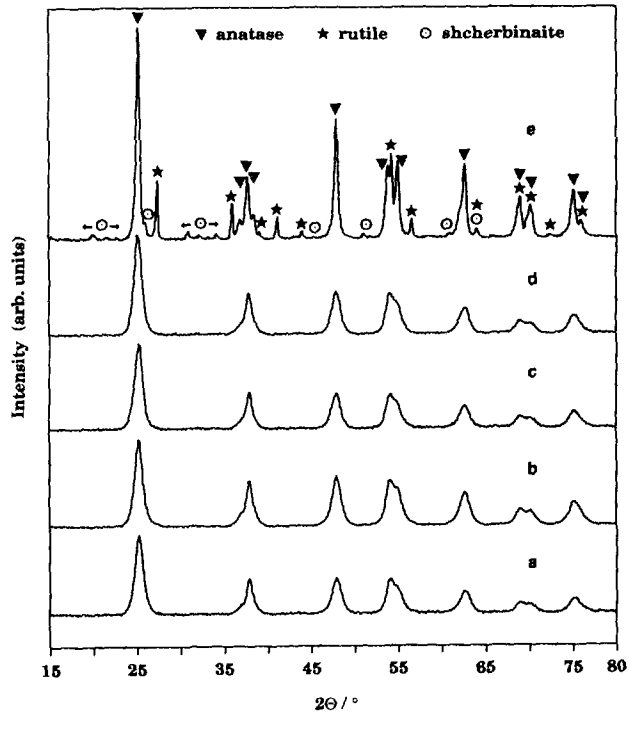

FIG. 3. X-ray diffraction patterns (Cu*K*α) of the V20*STA* series calcined at different temperatures in air: (a) raw, (b) 573 K, (c) 623 K, (d) 673 K, (e) 723 K. ▼, Anatase; ★, rutile; ⊙, shcherbinaite.

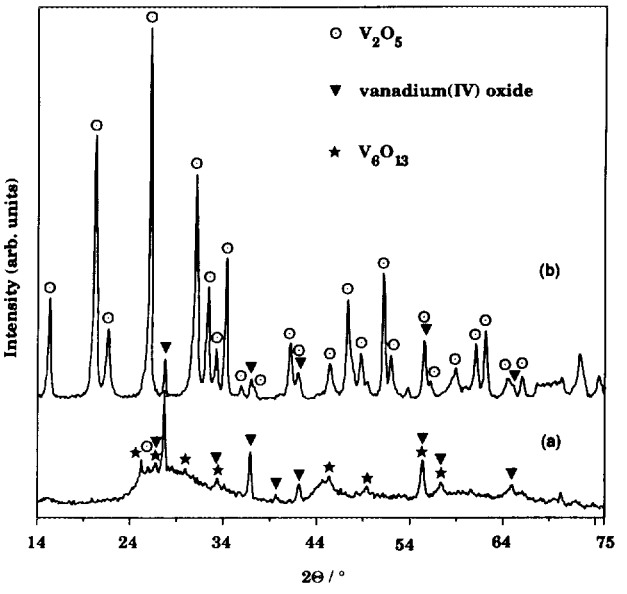

FIG. 4. X-ray diffraction patterns (Cu$K\alpha$, scintillation counter) of the vanadia aerogel *V*100: (a) raw, (b) calcined at 573 K. ▼, Vanadium(IV) oxide (most likely VO_2 and/or V_2O_4); ★, V_6O_{13}; ⊙, V_2O_5.

veals additionally that these building blocks are mostly anatase single crystals, as determined from the anatase lattice fringe spacings for the (101) reflection (0.352 nm). Besides the crystalline sectors, more diffuse parts can be seen, suggestive of amorphous or poorly crystalline regions. The primary particle diameters of titania lie between 5 and 11 nm, being in good agreement with the corresponding mean crystallite sizes derived from XRD. With respect to the vanadia component (0 wt% 'V_2O_5' in *V*0, 20 wt% in V20*STA*), the TEM images provide no indication of the presence of the vanadia phase in some long-range ordered state (small crystallites, multilayers on the anatase crystallites), suggesting remarkably high dispersion of the vanadia constituent.

Thermal analysis. Thermal analysis was performed in flowing air with a heating rate of 10 K min^{-1}. The thermoanalytical results measured for the raw aerogel V20*STA* (standard synthesis) are depicted in Fig. 7, which is representative of most of the raw, binary aerogels with 20 wt% 'V_2O_5'. The weight loss originated from the oxidation of organic residues and predominantly from the evolution of water (desorption of physisorbed water, dehydroxylation), which was already present in the aerogels. This conclusion clearly emerges from relating the TG curve with the monitored ion intensities of $m/z(CO_2^+) = 44$ (CO_2) and $m/z(H_2O^+) = 18$ (water) (Fig. 7). The liberation of water, representatively displayed in Fig. 7, began at room temperature and reached a maximum at 488 K with a preceding shoulder at ca. 410 K. H_2O evolution at the beginning originated mainly from physisorbed water; at higher temperatures it was dominated by the contribution of water from the oxidation of organic contaminants. A broad three-step CO_2 evolution was detected, which started at ca. 370 K and attained a maximum at 508 K followed by two shoulders at higher temperatures. In accordance with these gravimetric results, the DTA curve is dominated by two broad exothermal peaks at 480 and 557 K followed by a minor shoulder, all three related to the corresponding oxidation of organic residues and concomitant formation of CO_2. The exothermal DTA peak at 793 K reflects crystallization of the vanadia component to V_2O_5, which later started to melt at ca. 910 K with the corresponding endothermal DTA peak at 946 K. At ca. 670 K the reoxidation of the partly reduced vanadia component, related to the weight uptake and indicated by the TG curve, began to dominate over CO_2 and H_2O evolution.

The binary aerogels with 20 wt% 'V_2O_5', calcined at 573 K in air (standard calcination) showed virtually the same thermoanalytical characteristics as the corresponding raw (original) aerogels. Exothermal CO_2 evolution extended from ca. 470 to 770 K, which shows that despite the calcination at 573 K for 5 h, a considerable amount of organic residues persists in the aerogels. These organic residues are ≤0.1 wt% carbon, compared with ca. 2 wt% in the raw samples (Table 3). H_2O evolution was found to take place from ca. 300 to 850 K and was dominated mainly by the endothermal desorption of physisorbed water. Crystallization of V_2O_5 was reflected by an exothermal double peak at 780–800 and 805–840 K, respectively. Endothermal melting of V_2O_5 began at ca. 910 K and revealed a maximum at ca. 950 K. However, the weight increase due to oxidation of the vanadia component was still apparent despite the calcination at 573 K. The appropriate weight gain began at ca. 670 K. Besides the green-brown color of the aerogel samples after calcination at 573 K, such a weight uptake further indicates that the vanadia component is still present in a partly reduced state. Although the weight uptakes of 0.44–0.65 wt% are superimposed by CO_2 and H_2O evolution, they are suggestive of a theoretical stoichiometry V_3O_7, which is based on a theoretical uptake of 0.606 wt% for the oxidation of V_3O_7 to V_2O_5 (referred to 20 wt% 'V_2O_5').

The traces of CO_2 and H_2O evolution of the raw aerogel V20*STA* and portions of this material calcined in air at 573–723 K are summarized in Fig. 8. The content of organic contaminants decreased with increasing calcination temperature, but some residues were still present even after calcination at 723 K. The maxima of CO_2 evolution of the calcined samples were shifted to ca. 600 K (Fig. 8). Moreover, a shallow second stage occurred at ca. 790 K, indicative of the restructuring due to crystallization of V_2O_5 and concomitant partial phase transformation of anatase to rutile (Figs. 8a–d). Consequently, the associ-

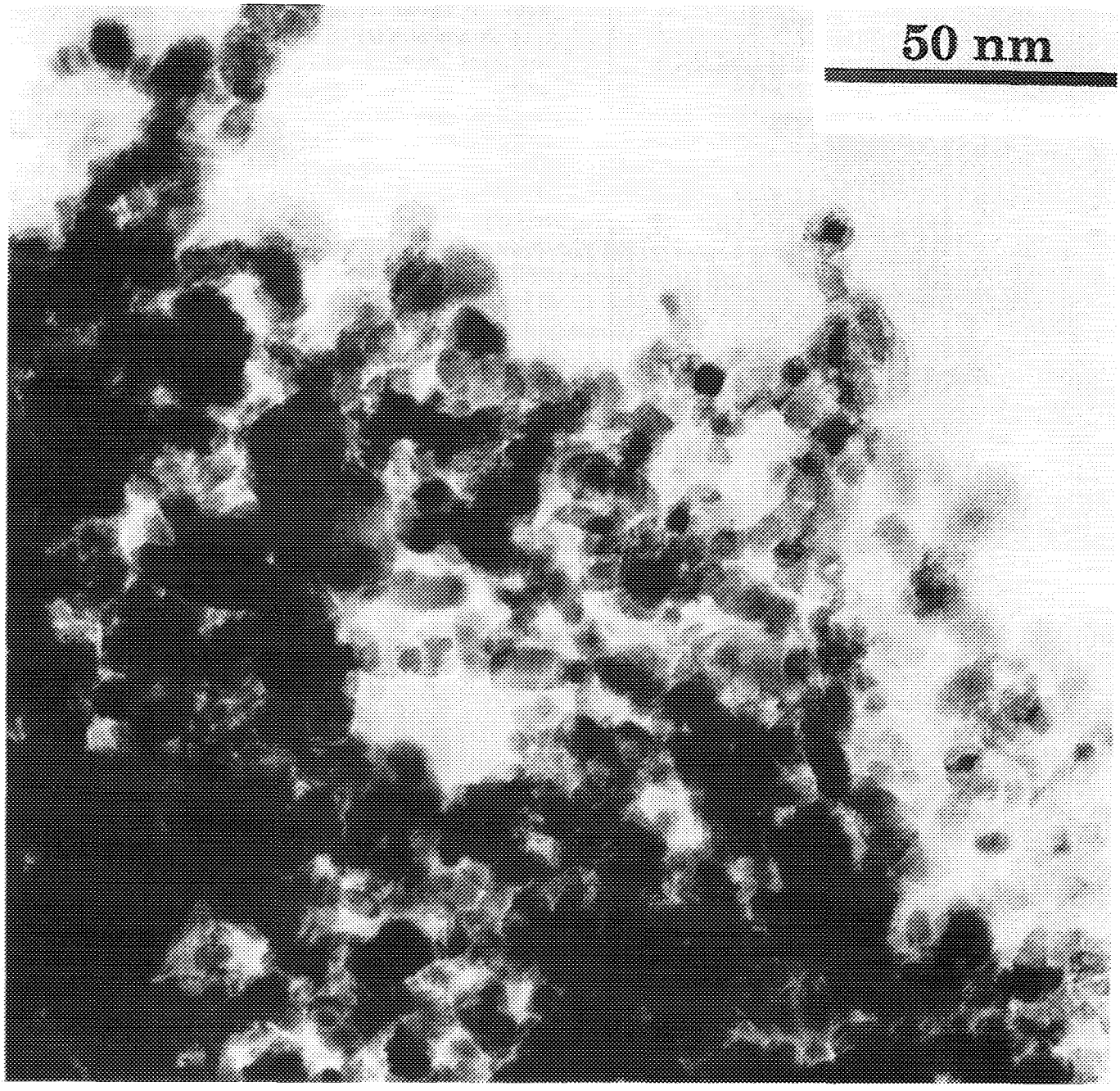

FIG. 5. Diffraction-contrast TEM image of aerogel V20*STA* calcined at 573 K in air (standard).

ated organic residues are not completely removable without major changes of the structural properties. It emerges from the H_2O evolution that the amount of physisorbed water is comparable for both the raw aerogel and the samples calcined up to 673 K, all reaching a maximum at ca. 395 K (Fig. 8). Only the sample calcined at 723 K with a concomitant decrease in the specific surface area has significantly suppressed water adsorption capacity.

The thermoanalytical behavior of V20*H2SO4*, synthesized with sulfuric acid and calcined at 573 K, is illustrated in Fig. 9a. Apart from the traces of H_2O and CO_2 evolution, which are comparable to those of the other equally calcined aerogel samples (Fig. 8), the trace for SO_2 ($m/z = 64$) with a maximum at ca. 830 K reveals the oxidation of sulfur-containing residues. This behavior emerges from the marked weight loss starting around 730 K and the

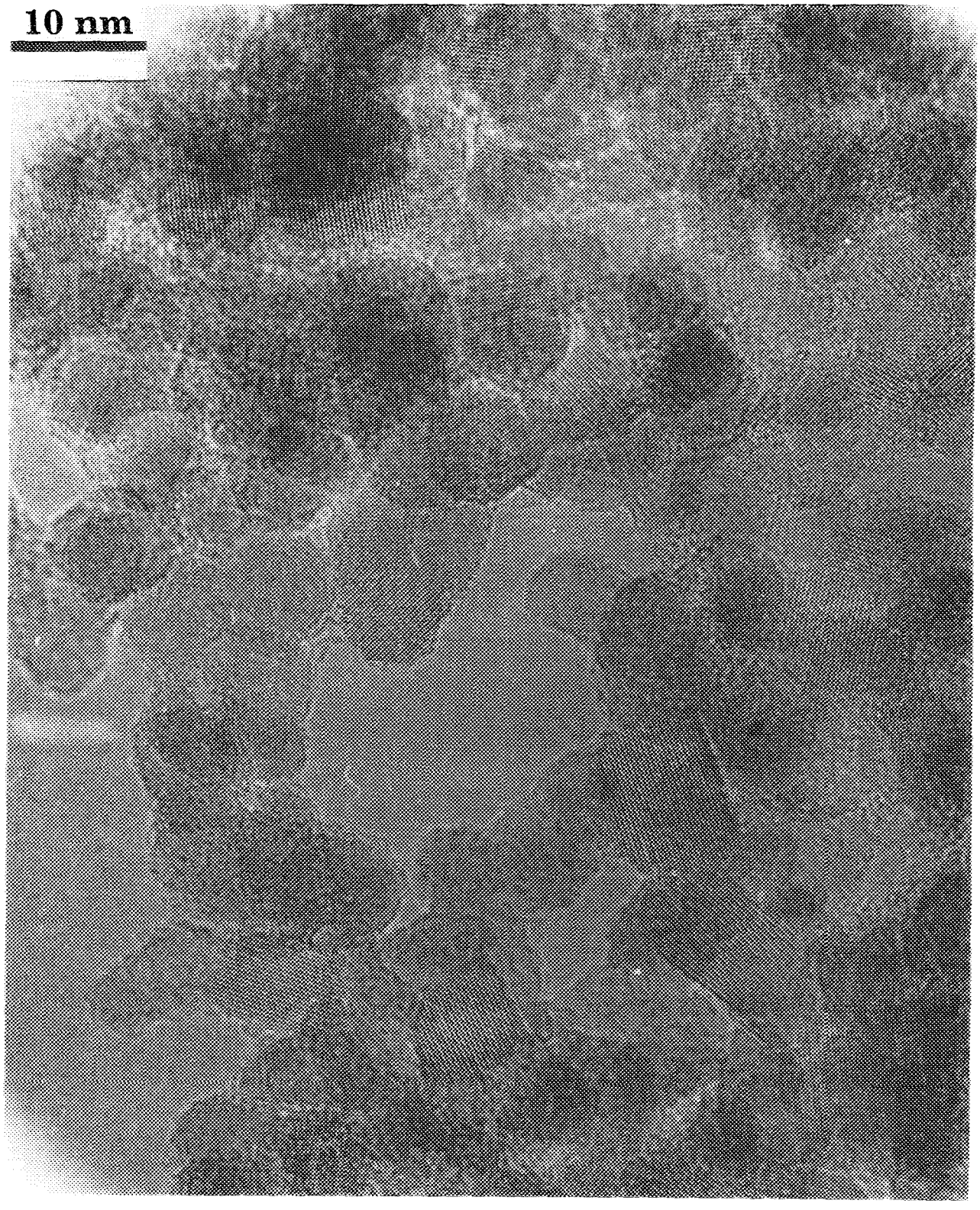

FIG. 6. High-resolution transmission electron micrograph of aerogel V20*STA* calcined at 573 K in air (standard).

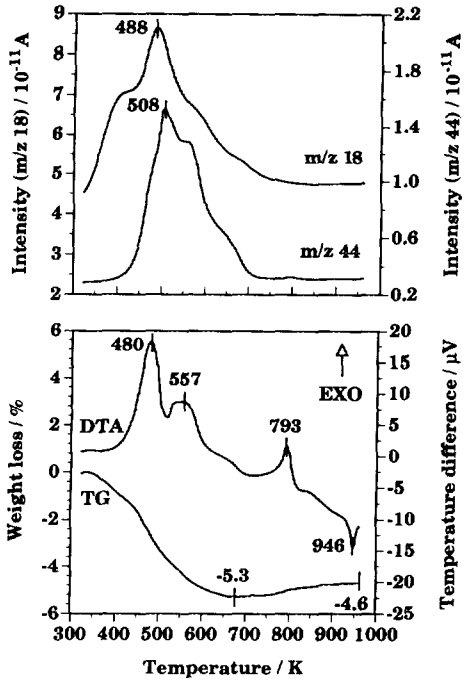

FIG. 7. Thermoanalytical investigation of the raw aerogel V20*STA*. Bottom: TG and DTA curves; top: ion intensities of $m/z(CO_2^+) = 44$ (CO_2) and $m/z(H_2O^+) = 18$ (water). Heating rate: 10 K min^{-1}, air flow: 25 ml min^{-1}.

broad exothermal DTA signal with a maximum at 835 K. The concomitant shallow maximum in CO_2 evolution (Fig. 9a) indicates a restructuring of the solid, which may imply that the mentioned sulfuric residues are partly trapped in the solid. In addition, the above-mentioned crystallization of the vanadia constituent (ca. 800 K) must be taken into account. The sulfuric contaminants obviously originate from the sulfuric acid used for the sol–gel preparation, which persisted in the sol–gel product (40) and was reduced during supercritical drying. This reduction manifested as a slightly increased final pressure of 26 MPa, suggestive of the production of volatile sulfuric compounds (H_2S). Moreover, sulfur deposits were observed inside the autoclave. When compared with the nominal sulfur content of 2.56 wt%, the amount of sulfur in the raw aerogel (derived from elemental microanalysis) amounts to 2.1 wt%, which confirms that part of the sulfur must have been lost during SCD.

Thermoanalytical results for the raw vanadia aerogel V100 are depicted in Fig. 9b. H_2O evolution occurred at ca. 300 K and reached a maximum at 380 K. CO_2 evolution started at ca. 370 K and reached a maximum at 560 K, which was consistent with the exothermal DTA peak at 560 K. This exothermicity was superimposed by the exothermal oxidation–crystallization of the reduced vanadia component. The corresponding weight uptake became dominant at ca. 500 K and provided further evidence for the reduced oxidation state, as already illustrated in Fig. 4 (pattern a).

The carbon content of the majority of raw vanadia–titania aerogels ranges from 2 to 2.8 wt%, as derived from elemental microanalysis. These organic residues are attributed mainly to the realkoxylation of surface hydroxyl groups during SCD (4, 41). Probably to a small extent, some unhydrolyzed, incorporated alkoxide ligands must also be taken into account. The lower carbon contents of raw V20*SGT*323, V20*H2SO4*, and *V*100 can be attributed to enhanced hydrolysis conditions, which are represented by the highest sol–gel temperature, the double protonic acid H_2SO_4, and the highest hydrolysis level, respectively. With *V*100 an additional effect is based most likely on some competitive hydroxylation of the oxidic surface due to the large amount of water used (see Experimental) during SCD. In essence, all aerogels contain a considerable amount of organic residues after high-temperature SCD, which persists partly even after calcination at 723 K.

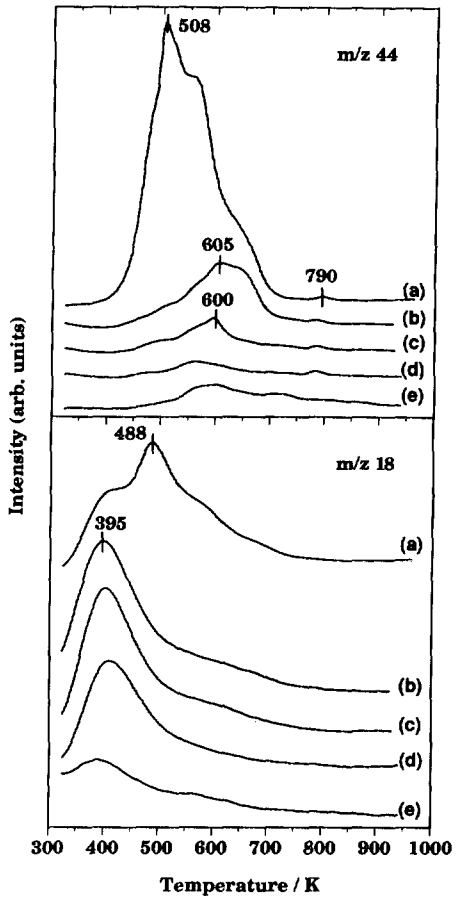

FIG. 8. CO_2 evolution (top) and H_2O evolution (bottom) during thermoanalytical runs of V20*STA* catalysts calcined at different temperatures in air: (a) raw, (b) 573 K, (c) 623 K, (d) 673 K, (e) 723 K. Heating rate: 10 K min^{-1}; air flow: 25 ml min^{-1}.

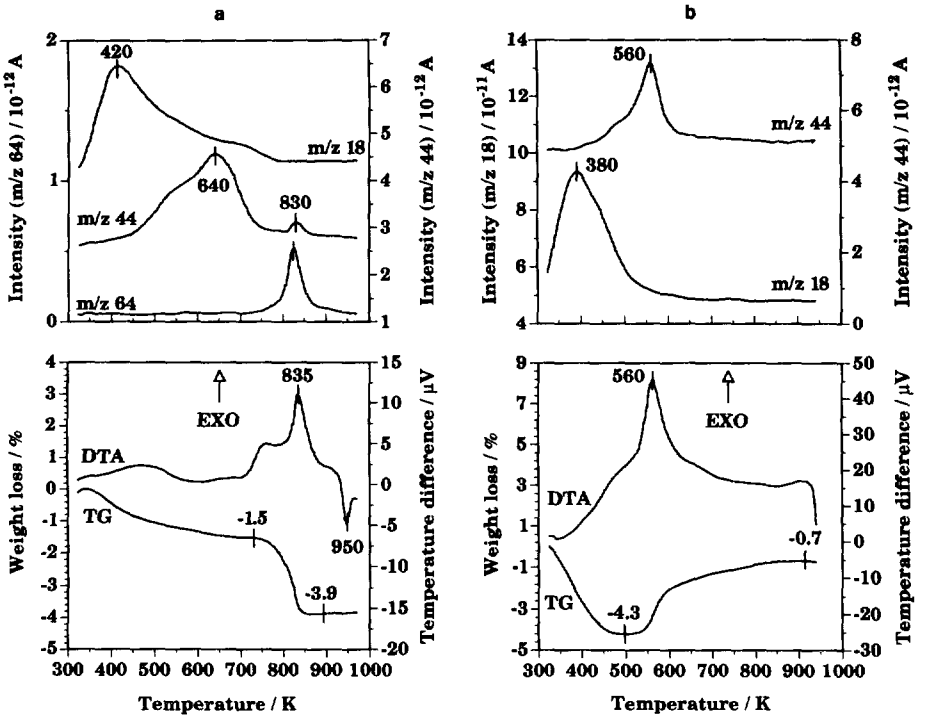

FIG. 9. Thermoanalytical investigations of aerogels (a) V20*H2SO4* calcined in air at 573 K and (b) *V*100 raw. Bottom: TG and DTA curves; top: ion intensities of $m/z(SO_2^+) = 64$, $m/z(CO_2^+) = 44$ (CO_2), and $m/z(H_2O^+) = 18$ (water). Full range for m/z 18 in (a) corresponds to 1–7 × 10^{-11} A, and for the other masses, as indicated in the figure. Heating rate: 10 K min^{-1}; air flow: 25 ml min^{-1}.

Selective Catalytic Reduction of NO by NH_3

Specific and overall activities are summarized in Table 4. Note that the specific activities at 423 K were compared on the basis of turnover frequency [TOF in (mol NO) (mol V)$^{-1}$ s^{-1}], reaction rates per BET surface area [(mol NO) m^{-2} s^{-1}] as well as reaction rates per gram of catalyst [(mol NO) $(g_{cat})^{-1}$ s^{-1}]. TOF values were calculated on the basis of nominal, molar loadings of vanadium, as noted under Experimental. Since it is very likely that a part of the vanadium species is not accessible to the reactant gases, such TOF data represent "conservative" estimates of intrinsic TOF values. Therefore, the term 'TOF' is used with single quotation marks throughout this work. It is obvious that the BET surface area (S_{BET}) is not a selective measure of the vanadia surface area (surface vanadia sites are not selectively titrated). Yet if we assume that the compositional and chemical effects on the active sites are represented by the 'TOF' value, then the S_{BET}-related reaction rate (r_s) should lend itself to reasonable estimates of changes in vanadia dispersity. As a measure of overall activity, the temperature necessary for 50% NO conversion ($T_{50\%}$) under standard conditions was quoted.

It emerges from Table 4 that the majority of the vanadia–titania aerogel catalysts with 20 wt% 'V_2O_5' loading (calcined at 573 K) reached 50% NO conversion at 434–439 K. Only V20*H2SO4*, which contains a considerable amount of sulfuric contaminants (sulfuric acid as sol–gel catalyst), attains $T_{50\%}$ at 468 K.

Typical NO and NH_3 conversion plots of the loading series *V*0 to *V*100, all calcined at 573 K, are depicted in Fig. 10. The overall activity increases distinctly with increasing loading from 0 to 30 wt% 'V_2O_5' (Fig. 10, Table 4). Note that the integral reactor test of *V*100 was performed with 118 mg instead of the 44 mg used for other catalysts of the loading series. NH_3 conversions were generally up to 5% higher than NO conversions at higher temperatures due to a small loss to direct oxidation.

With the most active catalysts this oxidation generally occurred at ca. 470 K and seemed to stay at a constant level up to 558 K (the highest temperature used in the integral reactor test). N_2O production was also minimal and became apparent beyond ca. 510 K. It reached concentrations of several vppm, which were close to the detection limit of N_2O.

Arrhenius plots of the vanadia loading series in Fig. 11 reflect that the specific activity per overall vanadium ('TOF') increases significantly with increasing loading. The highest 'TOF' obtained among all aerogels is comparable to that of a multiply grafted vanadia on titania catalyst, which possesses a high vanadia dispersion (7) (Table 4, Fig. 11). Comparison of 'TOFs' with reaction rates per BET surface area at 423 K (Table 4) suggests that two

TABLE 4

Selective Catalytic Reduction of NO by NH_3

Aerogel	'TOF'[a] × 10^4 (mol NO/mol V/s)	$r_s \times 10^9$ (mol/m^2/s)	$r_w \times 10^7$ (mol/g_{cat}/s)	E_a (kJ/mol)	$T_{50\%}$ (K)
V20*STA*	1.4	1.6	3.0	59	435
V20*STA*623	1.4	1.5	3.0	60	436
V20*STA*673	1.7	2.1	3.6	60	429
V20*STA*723	0.9	4.8	2.0	57	431[b]
V20*ViP*	1.4	1.9	3.0	60	437
V20*SGT*273	1.3	1.7	2.9	60	437
V20*SGT*323	1.4	1.7	3.2	58	434
V20*H2SO4*	0.4	0.6	0.8	65	468
*V*0	—	—	—	—	—
*V*5	0.4	0.1	0.2	66	520[b]
*V*10	0.7	0.4	0.7	59	469
*V*30	2.4	4.0	7.8	55	414
*V*100	0.2	8.7	2.2	44	430[b]
*V*20*HR*8	1.4	2.0	3.0	61	436
*V*20*HR*30	1.4	1.6	3.2	58	434
*V*20*HR*120	1.4	1.8	3.2	61	436
V20*PR*30	1.4	1.5	3.1	60	436
V20*PR*12	1.3	1.4	2.8	58	438
V20*EM*0	1.5	1.6	3.3	60	435
V20*NP*10	1.5	1.5	3.2	58	435
Ti-3V[c]	2.7	2.0	0.6	43	410
Tigel-2V[d]	2.7	1.5	1.2	—	—
VTi Gel[e]	1.0	4.5	6.1	49	—
Pat[c]	1.7	1.2	0.8	43	397

Note. The kinetic data measured at 423 K are represented as turnover frequency ('TOF'), reaction rate per BET surface area (r_s), reaction rate per gram of catalyst (r_w), and apparent activation energy (E_a). Results of integral reactor tests are represented as temperature necessary to reach 50% NO conversion.

[a] Reaction rate referred to the designed vanadium content ('TOF') on the basis of the assumption that all vanadium species are accessible to the reactant gases.

[b] V20*STA*723: 78 mg_{cat}; *V*5: 184 mg_{cat}, 0.524 cm^3 (V_{cat}), differential reactor testing GHSV 8400–24,000 h^{-1}; *V*100: 118 mg_{cat}; otherwise as specified under Experimental.

[c] From Ref. (7) with the same experimental conditions except for GHSV (9000 h^{-1}): Ti-3V, vanadia grafted on P25 (Degussa) with 1.8 wt% 'V_2O_5', 27 m^2 g^{-1}, 1 g_{cat}; Pat, vanadia–titania prepared by sequential precipitation based on the Mitsubishi patent (10) with 4.8 wt% 'V_2O_5', 67 m^2 g^{-1}, 1 g_{cat}.

[d] From Ref. (42) with the same experimental conditions: Tigel-2V, vanadia grafted on titania xerogel with 4.4 wt% 'V_2O_5', 86 m^2 g^{-1}, 0.1 g_{cat}.

[e] From Ref. (12) with the same experimental conditions: VTi Gel in situ 513 K, vanadia–titania xerogel prepared by a two-stage sol–gel process with 53 wt% 'V_2O_5', 139 m^2 g^{-1}, 0.1 g_{cat}.

effects are likely to be discernible due to the loading increase. The increase in 'TOF' involves some desired chemical and/or compositional changes of the active vanadia sites (42, 43), which is consistent with the decline in the apparent activation energies from 66 to 55 kJ mol^{-1} (Table 4). However, this beneficial effect is not sufficient to explain the much more pronounced increase in reaction rates per BET surface area (Table 4). Considering the comparable S_{BET} within the loading series (*V*0–*V*30) and the above-mentioned assumptions, the second beneficial effect is supposed to be a concomitant significant increase in vanadia dispersion. The markedly lower 'TOF' of crystalline V_2O_5 (*V*100 calcined at 573 K) is attributed to the poor accessibility of the vanadium species. However, the reaction rate per S_{BET}, which represents the more appropriate estimate of accessible vanadium sites in this case, is by far the highest for crystalline V_2O_5 (Table 4) (12). This behavior is further supported by a more reliable

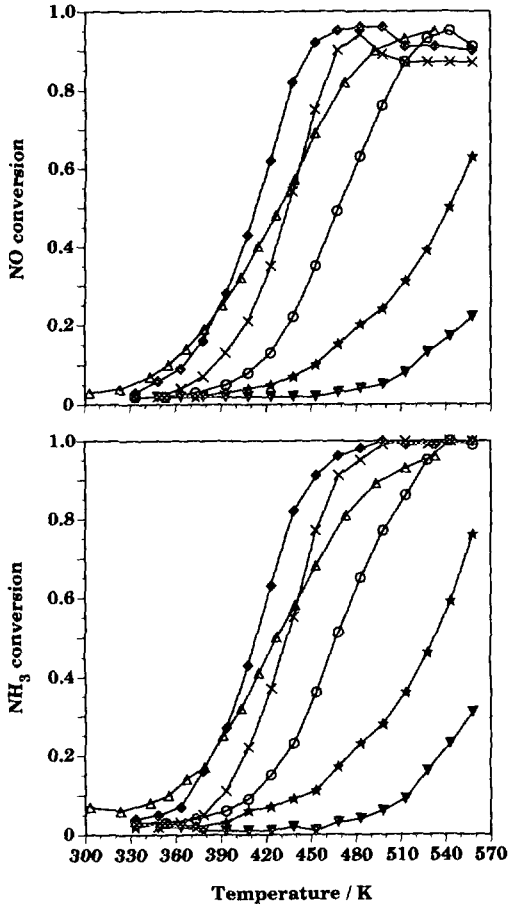

FIG. 10. Plots of conversion of the vanadia loading series for the reduction of NO by NH_3. Top: NO conversion; bottom: NH_3 conversion. ▼, *V0*; ★, *V5*; ⊙, *V10*; X, *V20*; ◆, *V30*, △, *V100*. Catalyst designations are explained in Table 1.

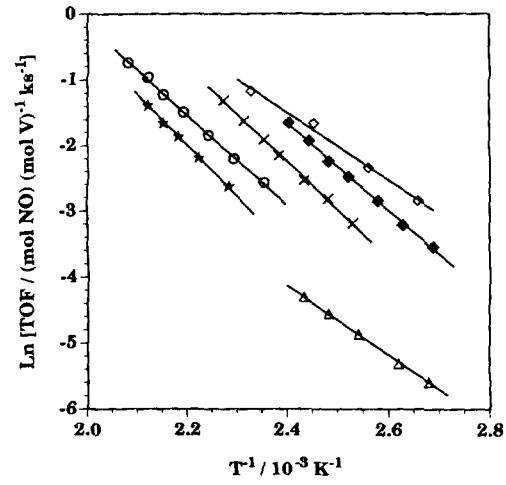

FIG. 11. Arrhenius plots of specific reaction rates of the vanadia loading series for the reduction of NO by NH_3. ★, *V5*; ⊙, *V10*; X, *V20*; ◆, *V30*; △, *V100*; ◇, Ti-3V for comparison from Ref. (7). Catalyst designations are explained in Table 1.

'TOF' calculation for the vanadia aerogel *V100*. For this purpose the number of accessible surface sites was estimated from the measured BET surface area and an assumed surface density of 4.87 V=O sites per square nanometer (30). The corresponding 'TOF' for V100 calcined at 573 K amounts thus to ca. 11×10^{-4} s^{-1}, which is the highest 'TOF' value among all presented catalysts (Table 4). To preserve the high specific surface area, the raw vanadia aerogel was activated *in situ* under SCR reactant gases at 513 K (91 mg_{cat}). Although the structural properties remained unchanged, such activation did not lead to improved catalytic peformance. The lower reaction rate per BET surface area (3.0 compared with 8.7×10^{-9} mol m^{-2} s^{-1} for *V100* calcined at 573 K) indicates that crystalline vanadium(IV) oxide (most likely VO_2 and/or V_2O_4, main phase of the *in situ* pretreated *V100* sample) does not reach the high intrinsic activity of crystalline V_2O_5. Handy *et al.* (12) reported reaction rates per BET surface area and S_{BET}-related 'TOFs' of vanadia xerogels that are about three times higher than the values reported in this work. The apparent activation energies of the vanadia aerogel catalysts amounted to 44 kJ mol^{-1} and are in good agreement with those of the vanadia xerogels in Refs. (7, 12).

The catalytic effects of the calcination temperature are shown in Fig. 12 and listed in Table 4. Calcination up to 623 K did not lead to significant changes; however,

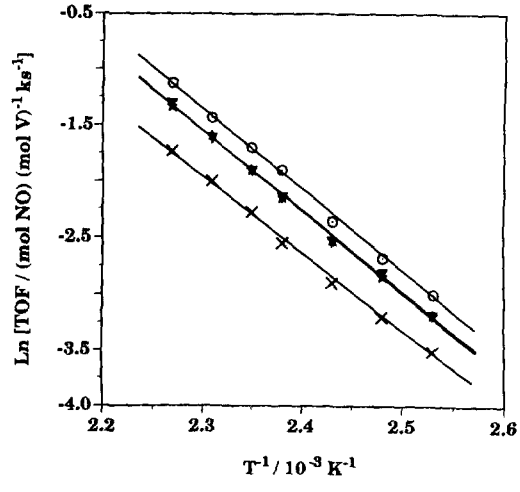

FIG. 12. Arrhenius plots of specific reaction rates of the V20*STA* series calcined at different temperatures for the reduction of NO by NH_3. ▼, V20*STA*; ★, V20*STA*623; ⊙, V20*STA*673; X, V20*STA*723. Catalyst designations are explained in Table 1.

calcination at 673 K revealed similar beneficial increases in both 'TOF' and reaction rate per S_{BET}, which indicates significant temperature-induced migration–agglomeration and/or partial removal of organic contaminants from the active vanadia surface fraction, as indicated in the section on thermal analysis and illustrated in Fig. 8. Both effects thus result in larger accessibility of the vanadia species. In contrast, the aerogel calcined at 723 K shows a marked decline in both 'TOF' and the reaction rate per gram of catalyst. This is interpreted in terms of the crystallization of vanadia to crystalline V_2O_5 and the concomitant decrease in S_{BET} (see XRD and physisorption studies above). Note, however, that the reaction rate per BET surface area shows a pronounced increase even surpassing the corresponding reaction rate of *V*30, again indicative of the high intrinsic activity of V_2O_5 (7, 12).

A comparison of the reaction rates per gram of catalyst reveals that the highest activity among the catalysts listed in Table 4 is obtained for *V*30 (30 wt% 'V_2O_5') calcined at 573 K. With the exception of V20*H2SO4* all vanadia–titania aerogels with 20 wt% 'V_2O_5' show comparable reaction rates per gram of catalyst, which of course parallels the fairly similar 'TOF' values (Table 4). Moreover, the apparent activation energies amounted to ca. 60 kJ mol^{-1}, which reflects again the marked similarity of the majority of vanadia–titania aerogels with a loading of 20 wt% 'V_2O_5' in the range of the preparation conditions investigated (Table 4).

DISCUSSION

As mentioned under Experimental, the preparation of the titania gels basically followed that of aerogel C in Ref. (20). In contrast to the previously reported titania aerogel, the titania aerogel prepared in this work (*V*0, Table 2) was redispersed at the gel stage using an additional amount of methanol, and the resulting sol was dried under supercritical conditions. Although the structure together with the macroscopic appearance of the sol–gel product was completely different [polymeric gel in (20), sol in this work], the properties of the dried titania aerogels were virtually identical. This essential finding rendered the homogeneous introduction of another component to the preformed "colloidally" distributed titania feasible and could thus be transferred to the preparation of multicomponent systems.

Within a wide range of investigated sol–gel and supercritical drying conditions, meso- to macroporous aerogels with high specific surface area were obtained in all cases (Fig. 1, Table 3). The porous structure results from the poorly defined morphology of these aerogel materials, which lends itself to loose packing configurations (Fig. 5). Moreover, these aerogel catalysts generally contain well-developed anatase crystallites in a fairly narrow size range (Fig. 3, Table 3). All binary aerogels calcined at 573 K did not show any evidence of long-range order of the vanadia constitutent (Figs. 3, 5, 6; Table 3). The comparable onsets of crystallization show that the relative stability of the vanadia component is very similar among the vanadia–titania catalysts examined. This behavior and the comparable catalytic performance (Table 4) imply a high dispersion, which remains largely uninfluenced by the majority of preparation conditions investigated (excluding the hydrolysis catalyst, calcination temperature, and loading discussed later). Similar findings have been reported by Wachs *et al.* (44), who suggested that loading and calcination temperature are among the most decisive factors that control the molecular design of an oxide–oxide catalyst. Considering the direct preparation method used,it is remarkable that within the wide range of conditions examined, the catalytic performance of the vanadia component remained virtually the same (Table 4). Structural evolution of the vanadia species with respect to dependence on the preparation conditions is reported in more detail in Part II of this study (45), which presents the data from the spectroscopic studies, including laser Raman, Fourier transform infrared, ^{51}V nuclear magnetic resonance, and secondary ion mass spectroscopy.

Only a few of the aerogels revealed significant morphological differences based on the synthesis procedure employed. Calcination of portions of V20*STA* showed that calcination in the range 573–673 K is dominated by some temperature-induced migration–agglomeration of the vanadia constituent and/or removal of part of the organic contaminants from the active vanadia surface fraction. These beneficial changes are reflected in the markedly increased 'TOF', reaction rate per BET surface area, and reaction rate per gram of catalyst of the V20*STA*673 catalyst calcined at 673 K (Table 4, Fig. 12). The occurrence of temperature-induced migration–agglomeration is supported by the results of our spectroscopic studies presented in Part II (45), which reflect an increasing contribution of oligomeric, ill-defined clusters covering and connecting the titania matrix. Thermoanalytical studies on the organic residues revealed that the content of organic contaminants decreases with increasing calcination temperature, but a minor part is still present even after calcination at 723 K (Fig. 8). In conjunction with X-ray diffraction studies, one can conclude that the organic contaminants are not completely removable without major changes in the structural and chemical properties of the aerogels (Figs. 3 and 8, Table 3). Note, however, that the appropriate CO_2 evolutions represent only integral data, which do not allow any assignment of the location of the evolved organic residues. Consequently, some uncertainty concerning the influence of the organic residues on the catalytic properties remains. At 723 K agglomeration–crystallization processes dominate, resulting in the appearance of crystalline V_2O_5 and the partial polymor-

phic transformation of anatase to rutile (Fig. 3e, Table 3). It is well known that this phase transition can be catalyzed in the presence of vanadia (35–37). This crystallization–transformation is clearly the reason for the decline in specific surface area as well as specific pore volume (Table 3). Due to the formation of bulk V_2O_5 the number of accessible vanadium sites decreases, which leads to a corresponding decline in the 'TOF' per overall vanadium (Table 4, Fig. 12).

The positive partial charge of titanium in the alkoxide precursor is significantly higher than that of vanadium in the related alkoxide (46), which enhances the sol–gel activity of titanium over vanadium. This property often results in a "core–shell" structure, with titania forming the "cores" in this case. Considering this behavior and the two-stage synthesis procedure applied (preformation of the titania matrix), it is likely that the (partly) hydrolyzed vanadium alkoxides react directly with the preformed titania-bound surface hydroxyl groups (heterocondensation), which leads to the high dispersion as well as accessibility of the vanadia component, as deduced from the good SCR activity obtained. Fourier transform infrared (FTIR) spectra of the OH stretching region, presented in Part II (45), provide clear evidence for a chemical reaction between the two components. Moreover, it is shown that for the higher concentrations of (partly) hydrolyzed vanadium alkoxide precursor, homocondensation of vanadium species (linking of adjacent V–OH groups) competes efficiently with anchoring at the remaining acidic Ti–OH groups. Consequently, vanadia clusters grow at the surface of the partly vanadia-covered titania matrix and/or in solution.

When vanadia nuclei are formed in the sol–gel solution (preferably by high nucleation rate), the ratio of homocoagulation to heterocoagulation of the vanadium oxo clusters becomes a decisive factor, which further influences the dispersion of the vanadia component. The acidic pH of the sol–gel solution should lead to positively charged titania particles and negatively charged vanadia clusters due to the distinctly different isoelectric points [pH_{pzc} (TiO_2) $\approx$ 4.5–6.3, pH_{pzc} (V_2O_5) = 1.4 (47)]. Thus, this property of the sol–gel solution should favor heterocoagulation processes of vanadia clusters.

In essence, the above-discussed sol–gel properties yield high dispersion as well as accessibility of the vanadia component, as inferred from the SCR data obtained (Table 4) and Raman spectroscopy (45).

The choice of vanadium oxide tri-*n*-propoxide for the standard vanadium alkoxide is based on its enhanced hydrolysis reactivity (high nucleation rate, high heterocondensation rate with titania-bound surface-hydroxyl groups) (15) combined with ease of handling. Steric factors exert the strongest influence on the hydrolytic stability of such alkoxide compounds. Introduction of an alkoxy group with a more complex structure retards the hydrolysis; the hydrolysis rate is lowered the most by branched alkoxy ligands (4, 15). When compared with the *n*-propoxy ligand, the isopropoxy group is thus more stable with respect to hydrolysis. However, this difference does not lead to significant changes in the catalytic activity.

Replacement of nitric acid with sulfuric acid showed two effects. Sulfuric acid is a very strong acid with two protons, which accelerates hydrolysis. Moreover, titanium(IV) forms hydrogen sulfate complexes in sulfuric acidic solution. This changed sol–gel activity might be the reason for the distinctly different textural properties (smaller S_{BET}, bimodal pore size distribution; Table 3, Fig. 2a) of the corresponding aerogel. The sulfate (complex) species are either adsorbed onto the surface or incorporated into the matrix, which results in deposition and/or inclusion (40) of sulfuric contaminants by reduction during supercritical drying (Table 3, Fig. 9a). The oxidation of these sulfuric residues occurs at ca. 730 K, as determined by thermal analysis of V20*H2SO4* calcined at 573 K (Fig. 9a). This persistence of the sulfuric contaminants up to high temperatures is a likely explanation for the significantly decreased catalytic performance of the aerogel catalyst V20*H2SO4* (Table 4). It is suggested that the sulfuric contaminants act as chemical and/or physical inhibitors of active vanadium sites, and can be removed in air only at elevated temperatures (ca. 700 K). However, such a calcination procedure would lead to significant structural changes, as presented for V20*STA*723 calcined at 723 K (Table 3, Fig. 3).

The textural and morphological properties remained largely unchanged on an increase in 'V_2O_5' loading up to 20 wt%. Only with *V*30 (30 wt% 'V_2O_5') were larger anatase crystallites observed to develop, suggestive of some enhanced crystal growth of anatase above a certain vanadium concentration. When compared with the structure sensitivity of multiply grafted vanadia/titania catalysts (7, 42), a comparably beneficial effect of increased vanadia content was observed with the vanadia–titania aerogels, which is represented by the increasing 'TOF' values at 423 K (Table 4, Fig. 11). The spectroscopic studies, presented in Part II (45), show that, up to a 'V_2O_5' content of 20 wt%, signals due to (V=O) stretching vibrations are detected only in the FTIR spectra. In general, the vanadia phase is present in the form of mostly amorphous patches, including small, ill-defined vanadia clusters. With increasing vanadia loading, amorphous vanadia layers cover and connect the titania matrix, until at the highest loading of 30 wt% 'V_2O_5' (*V*30), three-dimensional aggregates resembling crystalline V_2O_5 and two-dimensionally extended layer structures develop. The most active vanadia sites may thus be associated with two-dimensional disordered arrays of octahedrally bound vanadium oxo oligomers, as suggested in Refs. (42, 43). In addition,

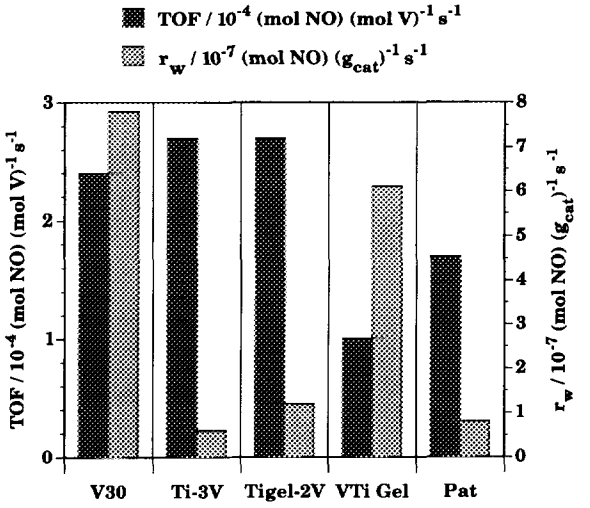

FIG. 13. Comparison of reaction rates referred to the vanadia content ('TOF') and reaction rates per gram of catalyst (r_w) of aerogel *V*30 calcined at 573 K (30 wt% 'V_2O_5') with corresponding literature data. Ti-3V, vanadia grafted on P25 (7); Tigel-2V, vanadia grafted on titania xerogel (42); VTi Gel, xerogel prepared by a two-stage sol–gel process (12); Pat, sequential precipitation according to the Mitsubishi patent (7, 10).

the much more pronounced increase in the S_{BET}-related reaction rates (Table 4) shows that besides this compositional-chemical effect, an increase in the vanadia dispersion is likely to occur.

Excellent vanadia dispersion on a high-surface-area titania matrix can be achieved by the direct preparation of both constitutents. This property enables the efficient use of a larger amount of accessible and active vanadium sites (Table 4). This beneficial property of vanadia–titania aerogels is illustrated in Fig. 13 by a comparison with literature data. The most active aerogel catalyst (*V*30 with 30 wt% 'V_2O_5') reaches an activity per vanadium atom similar to that of the well-dispersed multiply grafted catalysts (Ti-3V, Tigel-2V). However, due to high loading with excellent accessibility, the vanadia–titania aerogel possesses the highest activity per gram of catalyst.

The prominent effects of the heating rate during SCD are the drying rate and the time of exposure to elevated temperatures. The drying rate is crucial to hydrodynamic resistance and contact forces. These phenomena are known to have an impact on the concomitant differential drying forces (3, 5), which can affect the morphological and/or structural properties. In addition, the time of exposure to elevated temperatures influences various wet-chemical processes, including dissolution, reprecipitation, depolymerization, repolymerization, alkoxylation, and enhanced syneresis (network densification), leading to chemical and/or restructuring phenomena in such materials. The processes mentioned include some Ostwald ripening, coalescence–coarsening, sintering, and syneresis. However, within the range of heating rates examined a significant effect on the morphological and chemical properties was not evident (Table 3). Only with V20*HR*8, supercritically dried at 8 K h^{-1}, did the slightly lower S_{BET} of the vanadia–titania aerogel seem to be caused by the longer exposure to elevated temperatures.

V20*NP*10 supercritically dried with a nitrogen prepressure of 10 MPa shows the highest S_{BET} and specific pore volume among all catalysts studied in this work (Table 3). Apparently, these textural properties have to be attributed to a positive influence of nitrogen on solvent behavior (e.g., capillary forces), leading to reduced drying forces. This phenomenon merits further investigation.

CONCLUSIONS

The present study demonstrates that highly dispersed vanadia–titania aerogels with high acccessibility of the vanadia component can be synthesized by a two-stage sol–gel procedure with subsequent high-temperature supercritical drying. Within the range of preparation conditions investigated the properties of the titania matrix remain largely unchanged. A marked influence is observed only for the acid catalyst used in the sol–gel synthesis (nitric or sulfuric acid). In contrast, both the structural evolution and the dispersion of vanadia are predominantly influenced by the loading and the calcination temperature. Among the vanadia–titania aerogels prepared, samples with a loading of 30 wt% 'V_2O_5' exhibited the highest activity for the selective catalytic reduction of NO by NH_3. The reaction rate referred to the vanadium content ('TOF') is similar to that of highly dispersed, multiply grafted vanadia on titania catalysts, which indicates that vanadia, contained in the three-dimensional gel network, is well dispersed and exhibits SCR activity similar to that of multiply grafted vanadia species. The advantage of the aerogel catalysts resides in the higher vanadia loadings that can be achieved and, consequently, in higher reaction rates per catalyst weight.

ACKNOWLEDGMENTS

The authors acknowledge the assistance of R. Wessicken (ETH Zürich) with high-resolution transmission electron microscopy. This research was supported by a grant from the Nationaler Energie-Forschungs-Fonds (NEFF 569).

REFERENCES

1. Pajonk, G. M., *Appl. Catal.* **72,** 217 (1991).
2. Ko, E. I., *Chemtech* **23**(4), 31 (1993).
3. Schneider, M., and Baiker, A., *in* "Encyclopedia of Advanced Materials" (D. Bloor, R. J. Brook, M. C. Flemings, and S. Mahajan, Eds.), Vol. 1. Pergamon Press, Oxford, 1994.
4. Brinker, C. J., and Scherer, G. W., "Sol–Gel Science, the Physics

and Chemistry of Sol–Gel Processing." Academic Press, San Diego, 1990.
5. Scherer, G. W., *J. Am. Ceram. Soc.* **73,** 3 (1990).
6. Bond, G. C., and Tahir, S. F., *Appl. Catal.* **71,** 1 (1991).
7. Baiker, A., Dollenmeier, P., Glinski, M., and Reller, A., *Appl. Catal.* **35,** 351 (1987).
8. Baiker, A., Dollenmeier, P., and Glinski, M., U.S. Patent 4,789,533, Dec. 6, 1988.
9. Nickl, J., Dutoit, D., Baiker, A., Scharf, U., and Wokaun, A., *Appl. Catal. A* **98,** 173 (1993).
10. Watanabe, Y., Imanari, M., Takeuchi, M., Matsuda, S., Uno, S., Mori, T., and Nakajima, F., Japanese Patent 75 128,680, Oct. 9, 1975.
11. Pearson, I. M., Ryu, H., Wong, W. C., and Nobe, K., *Ind. Eng. Chem. Prod. Res. Dev.* **22,** 381 (1983).
12. Handy, B. E., Maciejewski, M., and Baiker, A., *J. Catal.* **134,** 75 (1992).
13. Livage, J., *Chem. Mater.* **3,** 578 (1991).
14. Nabavi, M., Sanchez, C., and Livage, J., *Eur. J. Solid State Inorg. Chem.* **28,** 1173 (1991).
15. Hirashima, H., Tsukimi, K., and Muratake, R., *J. Ceram. Soc. Japan Int. Ed.* **97,** 232 (1989).
16. Hirashima, H., Kamimura, S., Muratake, R., and Yoshida, T., *J. Non-Cryst. Solids* **100,** 394 (1988).
17. Hirashima, H., and Sudoh, K., *in* "Aerogels 3, Proceedings of the 3rd International Symposium on Aerogels, ISA-3, Würzburg 1991" (J. Fricke, Ed.), p. 51. North-Holland, Amsterdam, 1992.
18. Sudoh, K., and Hirashima, H., *J. Non-Cryst. Solids* **147/148,** 386 (1992).
19. Bosch, H., and Janssen, F., *Catal. Today* **2,** 1 (1987).
20. Schneider, M., and Baiker, A., *J. Mater. Chem.* **2,** 587 (1992).
21. Thermodynamics Research Center, Texas A&M University System, *in* "TRC Thermodynamic Tables—Non-Hydrocarbons," Vol. IV, p. i-5000. College Station, 1992.
22. Thermodynamics Research Center, Texas A&M University System, *in* "TRC Thermodynamic Tables—Non-Hydrocarbons," Vol. IV, p. i-30. College Station, 1992.
23. Mulder, C. A. M., and van Lierop, J. G., *in* "Aerogels, Proceedings of the 1st International Symposium on Aerogels, ISA1" (J. Fricke, Ed.). Springer Proceedings in Physics 6, p. 68. Springer, Berlin, 1986.
24. Barrett, E. P., Joyner, L. G., and Halenda, P. P., *J. Am. Chem. Soc.* **73,** 373 (1951).
25. Broekoff, J. C. P., *in* "Preparation of Heterogeneous Catalysts" (B. Delmon, P. Grange, P. Jacobs, and G. Poncelet, Eds.), p. 663. Elsevier, Amsterdam, 1979.
26. Harkins, W. D., and Jura, G., *J. Chem. Phys.* **11,** 431 (1943).
27. Klug, H. P., and Alexander, L. E., "X-Ray Diffraction Procedures for Polycrystalline and Amorphous Materials." John Wiley, New York, 1974.
28. JCPDS Mineral Powder Diffraction Data File 21-1272, Park Lane, PA.
29. JCPDS Mineral Powder Diffraction Data File 21-1276, Park Lane, PA.
30. JCPDS Mineral Powder Diffraction Data File 9-0387, Park Lane, PA.
31. Ehrenberger, F., "Quantitative, organische Elementaranalyse." VCH, Weinheim, 1991.
32. Weisz, P. B., and Prater, C. D., *Adv. Catal.* **6,** 143 (1954).
33. Schuck, G., Dietrich, W., and Fricke, J., *in* "Aerogels, Proceedings of the 1st International Symposium on Aerogels, ISA1" (J. Fricke, Ed.). Springer Proceedings in Physics 6, p. 142. Springer, Berlin, 1986.
34. Sing, K. S. W., Everett, D. H., Haul, R. A. W., Moscou, L., Pierotti, R. A., Rouquérol, J., and Siemieniewska, T., *Pure Appl. Chem.* **57,** 603 (1985).
35. Véjux, A., and Courtine, P., *J. Solid State Chem.* **23,** 93 (1978).
36. Bond, G. C., Sárkány, A. J., and Parfitt, G. D., *J. Catal.* **57,** 476 (1979).
37. Depero, L. E., Bonzi, P., Zocchi, M., Casale, C., and De Michele, G., *J. Mater. Res.* **8,** 2709 (1993).
38. JCPDS Mineral Powder Diffraction Data Files 9-0142 and 19-1398 Park Lane, PA.
39. JCPDS Mineral Powder Diffraction Data File 27-1318, Park Lane, PA.
40. Léaustic, A., and Riman, R. E., *J. Non-Cryst. Solids* **135,** 259 (1991).
41. Prassas, M., Phalippou, J., and Zarzycki, J., *J. Mater. Sci.* **19,** 1656 (1984).
42. Baiker, A., Handy, B., Nickl, J., Schraml-Marth, M., and Wokaun, A., *Catal. Lett.* **14,** 89 (1992).
43. Went, G. T., Leu, L.-J., Rosin, R. R., and Bell, A. T., *J. Catal.* **134,** 492 (1992).
44. Wachs, I. E., Deo, G., Kim, D. S., Vuurman, M. A., and Hu, H., *Stud. Surf. Sci. Catal.* **75A,** 543 (1993).
45. Scharf, U., Schneider, M., Baiker, A., and Wokaun, A., *J. Catal.*, **149,** 344–355 (1994).
46. Livage, J., *Prog. Solid State Chem.* **18,** 259 (1988).
47. Kung, H. H., *Stud. Surf. Sci. Catal.* **45,** 86 (1989).